INL/CON-07-12092
PREPRINT

# 3D CFD Model of High Temperature H2O/CO2 Co-electrolysis

## ANS Summer Meeting

Grant Hawkes
James O'Brien
Carl Stoots
Russell Jones

June 2007

The INL is a
U.S. Department of Energy
National Laboratory
operated by
Battelle Energy Alliance

# 3D CFD MODEL OF HIGH TEMPERATURE H2O/CO2 CO-ELECTROLYSIS

Grant Hawkes[1], James O'Brien[1], Carl Stoots[1], Russell Jones[2]

[1] *Idaho National Laboratory, Idaho Falls, Idaho,* grant.hawkes@inl.gov
[2] *Idaho State University, Idaho Falls, Idaho*

*A three-dimensional computational fluid dynamics (CFD) model has been created to model high-temperature co-electrolysis of steam and carbon dioxide in a planar solid oxide electrolyzer (SOE) using solid oxide fuel cell technology. A research program is under way at the Idaho National Laboratory (INL) to simultaneously address the research and scale-up issues associated with the implementation of planar solid-oxide electrolysis cell technology for syngas production from $CO_2$ and steam. The CFD model represents a single cell as it would exist in an electrolysis stack. Details of the model geometry are specific to a stack that was fabricated by Ceramatec , Inc. and tested at the Idaho National Laboratory. Mass, momentum, energy, and species conservation and transport are provided via the core features of the commercial CFD code FLUENT. A solid-oxide fuel cell (SOFC) model adds the electrochemical reactions and loss mechanisms and computation of the electric field throughout the cell. The FLUENT SOFC user-defined subroutine was modified to allow for operation in the SOEC mode. Model results provide detailed profiles of temperature, Nernst potential, operating potential, anode-side gas composition, cathode-side gas composition, current density and hydrogen production over a range of stack operating conditions. Mean CFD model results are shown to compare favorably with results obtained from a one-dimensional co-electrolysis model and with experimental results obtained from an actual ten-cell stack tested at INL over a range of operating conditions.*

## I. INTRODUCTION

The Idaho National Laboratory (INL), in conjunction with Ceramatec Inc. (Salt Lake City, USA) has been researching the use of solid-oxide fuel cell technology to electrolyze steam for large-scale nuclear-powered hydrogen production. A related experimental research project is now underway at the INL to demonstrate and evaluate the production of syngas by simultaneous high-temperature electrolysis of steam and carbon dioxide ($CO_2$) using solid oxide fuel cell technology [1,2]. A strong interest exists in the large-scale production of syn-gas from steam and $CO_2$ to be reformed into a usable transportation fuel. If biomass is used as the carbon source, and if the process is powered by nuclear energy, the overall process is climate neutral. With the price of oil currently around $60 / barrel, synthetically-derived hydrocarbon fuels (synfuels) have become economical. Synfuels are typically produced from syngas – hydrogen (H2) and carbon monoxide (CO) -- using the Fischer-Tropsch process, discovered by Germany before World War II. Traditionally, syngas has been produced via coal gasification, and more recently by steam reforming of natural gas. Both of these techniques consume non-renewables and emit greenhouse gases.

The INL high-temperature co-electrolysis program envisions using nuclear energy to power reversible solid-oxide fuel cells, electrolyzing steam and carbon dioxide ($CO_2$) simultaneously (Eq. 1):

$$H_2O + CO_2 \longrightarrow H_2 + CO + O_2 . \qquad (1)$$

Co-electrolysis, however, is significantly more complex than simple steam electrolysis. This is primarily due to the multiple reactions that occur: steam electrolysis, $CO_2$ electrolysis, and the water gas shift reaction (WGSR):

$$CO + H_2O \underset{k_b}{\overset{k_f}{\Leftrightarrow}} H_2 + CO_2 \qquad (2)$$

where $k_f$ and $k_b$ represent the forward and backward reaction rates. Reaction kinetics govern the relative contributions of these three reactions. It is also important to note that the electrolysis reactions are not equilibrium reactions since the electrolyte completely separates the products from the reactants. However, the WGSR is a kinetically fast, equilibrium reaction in the presence of a Ni catalyst at high temperature. Also, if the cell potential is high enough, CO can potentially be further electrolyzed to elemental C:

$$CO \rightarrow C + \frac{1}{2} O_2 \qquad (3)$$

producing solid particulates that can then deposit on cell surfaces, reducing cell performance.

Syngas could also be produced via separate electrolysis of steam and $CO_2$. There are, however, significant advantages to electrolyzing steam and $CO_2$ simultaneously. Focusing only upon the electrolysis step, co-electrolysis is more energy-efficient than separate electrolysis. For a given solid oxide electrolysis cell, $CO_2$ electrolysis will exhibit a higher area specific resistance (ASR) than for steam electrolysis. This is due to the

slower overall kinetics of $CO_2$ electrolysis and the higher overpotentials required. In co-electrolysis, the WGSR is relied upon for most of the CO production and therefore the overall electrical requirement is less. A second advantage is that in co-electrolysis the likelihood of producing carbon by electrolysis of CO is reduced.

Advanced high-temperature nuclear reactors have the potential for substantially increasing the efficiency of syn-gas production from CO2 and water, with no consumption of fossil fuels, and no production of greenhouse gases. Thermal $CO_2$-splitting and water splitting for syn-gas production can be accomplished via high-temperature electrolysis, using only high-temperature nuclear process heat and electricity.

## II. MODEL DESCRIPTION

Two CFD models and the one-dimensional chemical equilibrium co-electrolysis (CECM) model are described in this section. The first CFD model was created to compare to the CECM model assuming adiabatic electrolyzer operation. The purpose of the second CFD model is to replicate the conditions of test #1 from the experimental results of Ref. [3]. A photograph of the tested ten-cell co-electrolysis stack is presented in Figure 1.

### II.A. FLUENT CFD Model

A 3-D CFD model was developed using the FLUENT [5] code to simulate a single co-electrolysis cell as it would exist in the interior of multiple-cell stack.

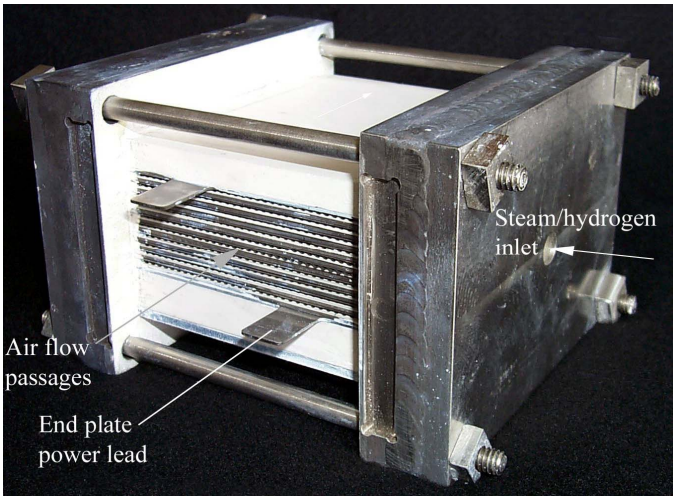


**Figure 1.** Detail of 10-cell SOEC stack.

This model is based on a planar solid oxide fuel cell stack similar to the stack described in Ref. [6]. This cell has an 8 cm x 8 cm active cell area. All properties and concepts are the same in this model as described in Ref. [6] with additional model details described below, with three exceptions: (1) only the active cell area with no edge rails is modeled, (2) the activation overpotential is zero, and (3) inlet and outlet regions allow for the shift reaction to reach equilibrium before entering or exiting the model.

Figure 2 shows the numerical mesh used with the different components. The mesh is 30 x 30 in the active cell area. Eight cells are used in the cross-flow stream for the current collectors. There are 116 cells in the inlet and

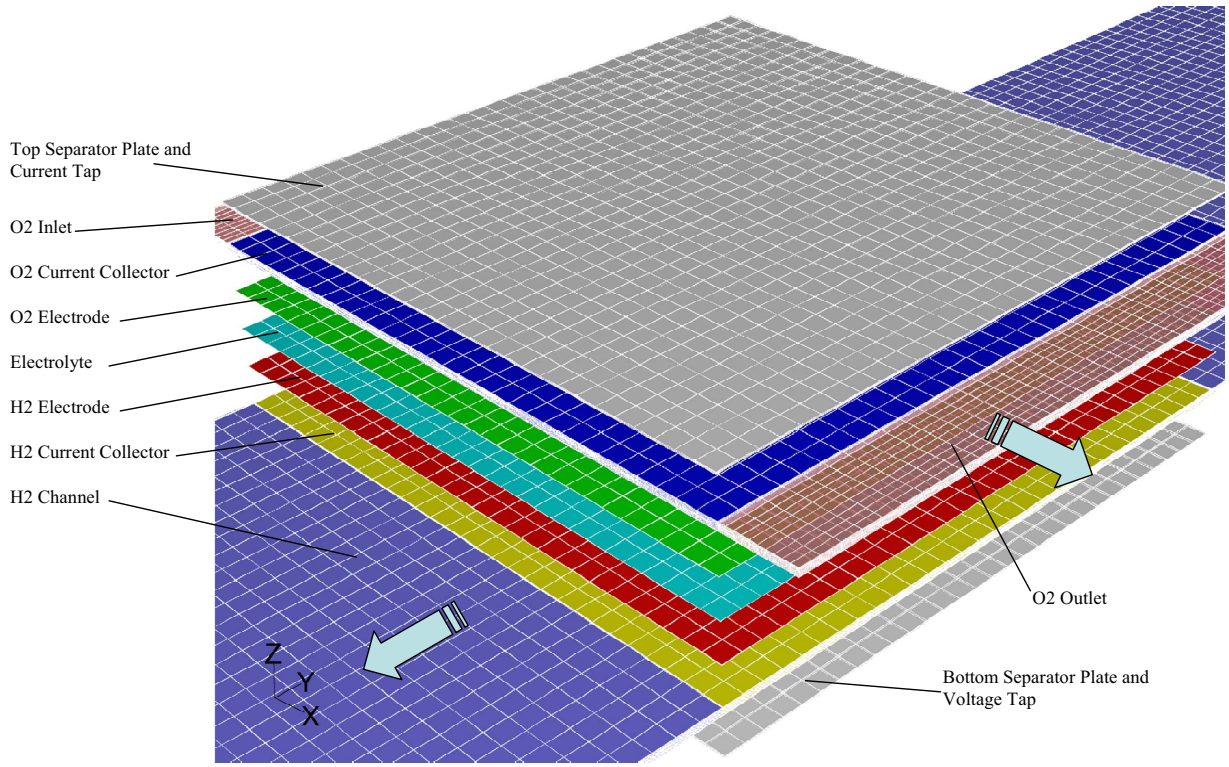


**Figure 2.** Mesh and model description of 8cm x 8cm active cell area.

outlet region of the process gas stream. Air sweep gas flows from - to + x, while the process gas stream flows from + to - y. In the experiment described in Ref. [3], the $H_2/CO_2/H_2O$ inlet process gas stream was heated in the oven in a circular tube before entering the inlet plenum. For the present CFD model, this heat-up length is modeled as a long flat duct with the same flow cross-sectional area as the flow channel inside the stack (1.02 mm x 80 mm). The entrance length is 35 cm and is modeled with two different wall boundary conditions on this inlet region. The first 20 cm is modeled as having a constant wall temperature boundary condition at 1073 K. The next 15 cm is modeled as adiabatic. Results indicate that the temperatures in this adiabatic region stay constant at 1073 K indicating that the shift reaction in Eq. (2) is at equilibrium before entering the adiabatic section. The flow then enters the active cell area where electrochemical reduction of the process gas occurs, producing $H_2$ and CO. The $O_2$ side has an inlet and outlet flow development length of 1 cm. A 15 cm process gas outlet flow length is modeled as adiabatic, followed by an additional 20 cm with three different heat transfer boundary conditions that will be discussed later. This outlet region is analogous to the flow exit tube carrying the products out of the oven.

Co-electrolysis of $H_2O$ and $CO_2$ was accomplished in FLUENT with the addition of a water gas shift (WGSR) reaction model. Experimental evidence shows that the reaction kinetics of steam electrolysis is much faster than that of the pure $CO_2$ electrolysis. These larger $CO_2$ molecules diffuse slower and create a concentration overpotential in the cell. For a given voltage, a lot more $H_2$ will be produced with $H_2O$ electrolysis compared to CO produced with pure $CO_2$ electrolysis. The area specific resistance (ASR) of a cell is closely related to the reaction kinetics. In one experimental test on a button cell, pure $H_2O$ electrolysis had an ASR of 0.59 Ω-cm$^2$. The inlet gas stream was immediately switched to pure $CO_2$; after switching the gas stream to pure $CO_2$ the ASR rose to 0.90. With the assumption the reaction rate for the WGSR is very fast (instantaneous) compared to pure $CO_2$ electrolysis, then this model that includes pure $H_2O$ electrolysis with the WGSR is a correct assumption. There is an advantage in power consumption to do co-electrolysis compared to pure $CO_2$ electrolysis, taking advantage of the WGSR. Two other advantages of co-electrolysis are that $H_2$ is less likely to leak, pure carbon is less likely to be produced. The FLUENT model has electrolysis occurring in the $H_2O$ with the WGSR occurring as shown in Eq. (2)

Forward and backward reaction rates at three different temperatures for SOFC are given by Ref. [7] as follows in Table I

TABLE I. Reaction rates for WGSR in SOFCs varying with temperature

| Temperature (K) | $k_f$ (kmole m$^{-3}$ Pa$^{-2}$ s$^{-1}$) | $k_b$ (kmole m$^{-3}$ Pa$^{-2}$ s$^{-1}$) |
|---|---|---|
| 1073 | 1.5 x $10^{-10}$ | 1.4 x $10^{-10}$ |
| 1123 | 3.2 x $10^{-10}$ | 3.5 x $10^{-10}$ |
| 1163 | 3.6 x $10^{-10}$ | 4.3 x $10^{-10}$ |

In order to predict the final composition as measured via an online micro gas chromatograph (GC) at ambient temperature in the experiment from Ref. [3], temperature-dependent reaction rates from the process temperature to ambient temperatures were needed. The temperature-dependent equilibrium constant, obtained from Ref. [8] is related to the forward and reverse reaction rates via:

$$K_{eq}(T)=\frac{k_f(T)}{k_b(T)} \tag{4}$$

For our analysis, $k_b$ from Table I was used along with Eq. (4) to determine $k_f$. Since $K_{eq}$ and $k_b$ are known, $k_f$ could be calculated, thus assuring that the $K_{eq}$ from [8] is satisfied. The net reaction rate (NRR) is defined as:

$$NRR = k_f P_{CO} P_{H2O} - k_b P_{CO2} P_{H2} \tag{5}$$

In FLUENT, the net rate of chemical reaction is calculated based on the molar concentration of reactants and products and not partial pressure of reactants and products as given in Eq. (5). To make the conversion, the ideal gas law is used as follows:

$$P=\frac{n}{V}RT \quad or \quad P=[C]RT \tag{6}$$

Now the NRR can be written as:

$$NRR = k_f (RT)^2 [C]_{CO}[C]_{H2O} - k_b (RT)^2 [C]_{CO2}[C]_{H2} \tag{7}$$

Yet in FLUENT the NRR is defined as:

$$NRR = k_{f\_FLUENT}[C]_{CO}[C]_{H2O} - k_{b\_FLUENT}[C]_{CO2}[C]_{H2} \tag{8}$$

then

$$\begin{aligned} k_{f\_FLUENT} &= k_f (RT)^2 \\ k_{b\_FLUENT} &= k_b (RT)^2 \end{aligned} \tag{9}$$

An exponential curve fit of $k_b$ versus 1/T from Table I yields:

$$k_b = 4.2475\,x10^4\, e^{\left(\frac{-1.5933\,x10^4}{T}\right)} \tag{10}$$

and applying Eq. (9) yields:

$$k_{b\_FLUENT} = 29359 T^2 e^{\left(\frac{-1.3247\,x10^8}{RT}\right)} \tag{11}$$

one can find $k_{f\_FLUENT}$ by doing an exponential curve fit of

$$k_{f\_FLUENT} = k_{b\_FLUENT}(T) K_{eq}(T) \tag{12}$$

versus 1/T which gives

$$k_{f\_FLUENT} = 390.96T^2 e^{\left(\frac{-9.363x10^7}{RT}\right)} \quad (13)$$

where the numerator inside the exponential in Eqs. (11) and (13) is the activation energy in (J/kgmol).

For the adiabatic model, gas inlet temperatures on the process gas side and air sweep side were set at 1073 K. The adiabatic model has the active cell area and all 35 cm of outlet region taken as adiabatic. The model used to correlate to the experiment has a radiation heat transfer coefficient around the outer periphery of the cell with an emissivity of 1.0. The outside perimeter is 40 cm in the experiment and 32 cm in this model. This was taken into account in the boundary condition for the model as:

$$h_r = \left(\frac{40}{32}\right)\sigma\varepsilon\left(T_w^2 + T_\infty^2\right)\left(T_w + T_\infty\right) \quad (14)$$

where σ is the Stefan-Boltzmann constant, ε is the emissivity, $T_w$ is the current collector and separation plate outer wall, and $T_\infty$ is the oven temperature taken at 1073 K. The top and bottom of the separator plates are taken as adiabatic, since the model represents a single interior cell in the stack.

The 15 cm in the process gas stream exiting the cell is taken as adiabatic, representing the tube exiting the oven. The last 20 cm is adiabatic for the adiabatic model, and has a variation of a fast cool down with a wall temperature set at 300 K or a slow cool down with h=0.5 W/m$^2$-K and $T_\infty$=300 K.

Table II shows inlet mole fractions and mass flow rates for the two models.

Table II. Inlet conditions for models.

| Mole Fractions | $yH_2O$ | $yH_2$ | $yCO_2$ | yCO | $yN_2$ |
|---|---|---|---|---|---|
| Adiabatic | 0.185 | 0.100 | 0.123 | 0.000 | 0.592 |
| Experiment | 0.155 | 0.102 | 0.124 | 0.000 | 0.619 |

| Mass Flow Rate (per cell) | process gas (kg/s) | air sweep (kg/s) |
|---|---|---|
| Adiabatic | 3.137e-5 | 4.555e-5 |
| Experiment | 9.340e-6 | 4.930e-6 |

A contact resistance for the experimental model was placed between each current collector and electrode. The final contact resistance value of 8.9e-5 Ω-m$^2$ was obtained empirically. Its value was chosen to match the slope on the V-i curve with the experimental data. Electrolyte resistivity was set constant at 0.1 Ω-m. This value is the typical resistivity value for ScSZ in the range of 1073 K. The FLUENT model was run at 85 kPa for all cases.

### II.B. 1-D Chemical Equilibrium Model

Results of the FLUENT co-electrolysis analysis can be compared to results obtained using a one-dimensional chemical equilibrium model. The one-dimensional model was developed for incorporation into a systems-analysis code for evaluating overall performance of large-scale co-electrolysis plants. Full details of the one-dimensional model and its incorporation into the systems code are available in [4]. An abbreviated description will be provided here.

The Nernst potential for the co-electrolysis system can be calculated as a function of temperature using the Nernst equation for either steam-hydrogen or for $CO_2$-CO, provided the equilibrium composition of the components is used in the evaluating the equation. Therefore, prior to applying the Nernst equation, the electrolyzer-inlet equilibrium composition must be determined at the operating temperature. Our chemical equilibrium co-electrolysis model (CECM) determines the equilibrium composition of the system as follows.

The overall shift reaction that occurs during heatup from the cold unmixed inlet conditions to the hot mixed pre-electrolyzer state can be represented as:

$$y_{0,CO}\,CO + y_{0,CO2}\,CO_2 + y_{0,H2}\,H_2 + y_{0,H2O}\,H_2O \rightarrow y_{1,CO}\,CO + y_{1,CO2}\,CO_2 + y_{1,H2}\,H_2 + y_{1,H2O}\,H_2O \quad (15)$$

where the $y_0$ values represent the cold inlet mole fractions of CO, $CO_2$, $H_2$, and $H_2O$, respectively, that are known from specification of the individual component inlet gas flow rates. The unknown hot equilibrium mole fractions of the four species at the electrolyzer temperature, prior to electrolysis, are represented by the $y_1$ values. Simultaneous solution of the three chemical balance equations for carbon, hydrogen, and oxygen corresponding to Eq. (15) and the equilibrium constant equation:

$$K_{eq}(T) = \frac{y_{1,CO2}\,y_{1,H2}}{y_{1,CO}\,y_{1,H2O}} \quad (16)$$

yields the hot inlet composition. Note that Eq. (16) is the inverse of Eq. (4).

Once the hot inlet equilibrium composition is determined, the open-cell Nernst potential can be calculated from:

$$V_N = \frac{-\Delta G_{f,H_2O}(T)}{2F} - \frac{R_u T}{2F}\ln\left[\left(\frac{y_{1,H2O}}{y_{1,H2}\,y_{O2}^{1/2}}\right)\left(\frac{P}{P_{std}}\right)^{-1/2}\right] \quad (17)$$

where $y_{O2}$ is the mole fraction of oxygen on the air-sweep side of the cells ($y_{O2}$ ~ 0.21).

The electrolyzer outlet composition (state 2) can be determined similarly, after accounting for electrochemical reduction of the system. The chemical balance equation for oxygen must be modified to account for oxygen removal from the $CO_2$/steam mixture:

$$y_{1,CO} + 2y_{1,CO2} + y_{1,H2O} = y_{2,CO} + 2y_{2,CO2} + y_{2,H2O} + \Delta n_O \quad (18)$$

where $\Delta n_O$ is the relative molar rate of monatomic oxygen removal from the $CO_2$/steam mixture given by:

$$\Delta n_O = \frac{I_e}{2F\dot{N}_{Tot}} \tag{19}$$

In this equation, $I_e$ is the total ionic current, $I_e = i \cdot A_{cell} \cdot N_{cells}$. $\dot{N}_{Tot}$ is the total molar flow rate on the $CO_2$/steam side, including any inert gas flows, and $F$ is the Faraday number.

In general, the electrolyzer outlet temperature is unknown. The magnitude of any temperature change associated with electrolyzer operation depends both on the operating conditions (operating voltage, inlet composition, gas flow rates, etc.) and on the thermal boundary condition. For adiabatic electrolyzer operation, the outlet temperature can be determined as a function of operating voltage from simultaneous solution of the energy equation (with $Q = 0$) and the chemical balance and equilibrium constant equations. Alternately, if isothermal operation is assumed, the outlet composition can be determined independently of the energy equation and the heat required to maintain isothermal operation can be calculated as a function of operating voltage.

For pure-steam or pure-$CO_2$ electrolysis, the thermal neutral voltage is given by

$$V_{tn,j}(T) = \frac{\Delta H_{R,j}(T)}{2F} \tag{20}$$

where $\Delta H_{R,j}(T)$ is the enthalpy of reaction for electrolysis of pure component j ($H_2O$ or $CO_2$) at temperature $T$. At 800°C, $V_{tn,H2O} = 1.29$ V and $V_{tn,CO2} = 1.46$ V. For co-electrolysis, the thermal neutral voltage can range anywhere between the respective pure-component values, depending on inlet composition, oxygen utilization, and temperature. There is no simple explicit relation for multi-component-electrolysis thermal neutral voltage. In general, the thermal neutral voltage for co-electrolysis will be closer to the pure-steam value if the inlet composition is dominated by steam and hydrogen. Conversely, if the inlet composition is dominated by $CO_2$ and CO, the co-electrolysis thermal neutral voltage will be closer to the pure-$CO_2$ value. At an operating temperature of 800°C, with syngas-production-relevant inlet compositions for co-electrolysis (i.e., ~2-to-1 steam/hydrogen vs $CO_2$), a thermal neutral voltage value of ~1.34 V is typical.

The energy equation for the co-electrolysis process can be written as:

$$\dot{Q} - \dot{W} = \sum_P \dot{N}_i[\Delta H^o_{f_i} + H_i(T_P) - H^o_i] - \sum_R \dot{N}_i[\Delta H^o_{f_i} + H_i(T_R) - H^o_i] \tag{21}$$

where $\dot{Q}$ is the external heat transfer rate to or from the electrolyzer, $\dot{W}$ is the rate of electrical work supplied to the electrolyzer, $\dot{N}_i$ is the molar flow rate of each reactant or product, $\Delta H^o_{f_i}$ is the standard-state enthalpy of formation of each reactant or product and $H_i(T) - H^o_i$ is the sensible enthalpy for each reactant or product. Applying the energy equation in this form, all reacting and non-reacting species in the inlet and outlet streams are accounted for, including inert gases, process steam, hydrogen (introduced to maintain reducing conditions on the steam/hydrogen electrode), $CO_2$, and any excess unreacted process gases.

In general, determination of the outlet temperature from Eq. (21) is an iterative process. The heat transferred during the process must first be specified (e.g., zero for the adiabatic case). The temperature-dependent enthalpy values of all species must be available from curve fits or some other data base. The cathode-side hot electrolyzer inlet flow rates of steam, hydrogen, $CO_2$, CO, and any inert carrier gases such as nitrogen (if applicable) are specified. The inlet flow rate of the sweep gas (e.g., air or steam) on the anode side must also be specified. At this point, the total electrolyzer-inlet enthalpy given by the second summation term on the right-hand side of Eq. (21) can be evaluated.

The current density, active cell area, and number of cells are then specified, yielding the total ionic current, $I_e = i \cdot A_{cell} \cdot N_{cells}$. The iterative solution process proceeds as follows. Based on a guessed value of electrolyzer outlet temperature, $T_P$, and the specified current, the electrolyzer outlet composition can be determined as described previously, allowing for evaluation of the total enthalpy of the products.

The remaining term in the energy equation is the electrical work, which is the product of the per-cell operating voltage and the total ionic current. The operating voltage corresponding to the specified current density is obtained from:

$$V_{op} = \bar{V}_{Nernst} + i \times ASR(T) \tag{22}$$

The stack area-specific resistance, $ASR(T)$, quantifies the loss mechanisms in the operating cell. It must be estimated and specified as a function of temperature. The operating-cell mean Nernst potential, $\bar{V}_{Nernst}$, accounting for the variation of gas composition and temperature across the operating cell, can be obtained from an integrated form of the steam-hydrogen-based (or the $CO_2$-CO-based) Nernst equation:

$$\bar{V}_{Nernst}(T_P) = \frac{1}{2F(T_P - T_R)(y_{2,O_2} - y_{1,O_2})[y_{2,H_2}(T_P) - y_{1,H_2}]} \times \int_{T_R}^{T_P} \int_{y_{1,O2}}^{y_{2,O2}} \int_{y_{1,H2}}^{y_{2,H2}(T_P)} \Delta G_{R,H_2O}(T) + RT \ln\left(\frac{1 - y_{H_2} - y_{0,CO_2} - y_{N_2}}{y_{H_2} y_{O_2}^{1/2}}\right) dy_{H_2}\, dy_{O_2}\, dT \tag{23}$$

Note that the variable in this equation is the unknown product temperature, $T_P$. The steam mole fraction has been expressed in the integrand numerator in terms of the hydrogen mole fraction. The mole-fraction subscripts 0, 1, 2 again refer to the cold inlet, hot electrolyzer inlet, and the hot electrolyzer outlet states, respectively. Mole fractions at states 0 and 1 are fully defined. The state-2 mole fractions are based on the specified current density and the guessed value for $T_P$.

Once the mean Nernst potential is evaluated based on a guessed value for $T_P$, the operating voltage can be determined and the energy equation can be evaluated. The final converged solution for $T_P$ must simultaneously satisfy the chemical balance Eqs. for C, $H_2$, and $O_2$, the equilibrium constant Eq. (16), and the energy Eq. (21), subject to Eq. (22 – 23).

This model allows for accurate determination of co-electrolysis outlet temperature, composition (anode and cathode sides), mean Nernst potential, operating voltage and electrolyzer power based on specified inlet gas flow rates, heat loss or gain, current density, and cell *ASR(T)*. Alternately, for isothermal operation, it allows for determination of outlet composition, mean Nernst potential, operating voltage, electrolyzer power, and the isothermal heat requirement for specified inlet gas flow rates, operating temperature, current density and *ASR(T)*.

Predictions obtained from the 1-D integral model have been compared to results obtained from the 3-D FLUENT simulation as has been noted by the FLUENT adiabatic model. Results will be shown comparing these two models.

Calculated final equilibrium compositions have also been compared to experimental results obtained from both single-cell and co-electrolysis stack tests. Details of the experimental apparatus and results are provided in Refs. [3,4]. Comparisons to stack results will be presented here. Measurements of electrolyzer outlet composition were obtained with a downstream dewpoint sensor for steam and with a gas chromatograph for the other gases. However, since these downstream gas composition measurements were obtained at near-room temperatures, these measured compositions are not necessarily expected to agree with predicted outlet compositions evaluated at the furnace temperature. During cool-down from the furnace temperature to room temperature, the gas composition can change, in accordance with the temperature dependence of the shift-reaction equilibrium constant. The magnitude of the composition shift is dependent on cooling rate, presence or absence of catalyst, etc. In general, rapid cooling yields cold outlet compositions that are close to the hot outlet values. These kinetic effects were included in the FLUENT model by varying the cooling rate of the outlet gas flows in the downstream channel.

## III. RESULTS

Results of the FLUENT and 1-D model simulations obtained for various cases are presented in Figures 3 through 11.

### III.A. FLUENT and 1-D Adiabatic Results

Comparisons of the FLUENT model and the 1-D model for the adiabatic case with a constant *ASR* value of 1.5 $\Omega \cdot cm^2$ are shown in Figures 3 through 7. Figure 3 shows a comparison of predicted per-cell operating voltage versus current density polarization curves for the FLUENT model and 1-D model. The mean Nernst potential predicted by the two models is also shown as a function of current density. The mean Nernst potential for the CFD model is a two-dimensional average over the face of the electrolyte that includes the effects of the cross-flow geometry of the process gases and the sweep gas. Nevertheless, both sets of curves are essentially on top of each other.

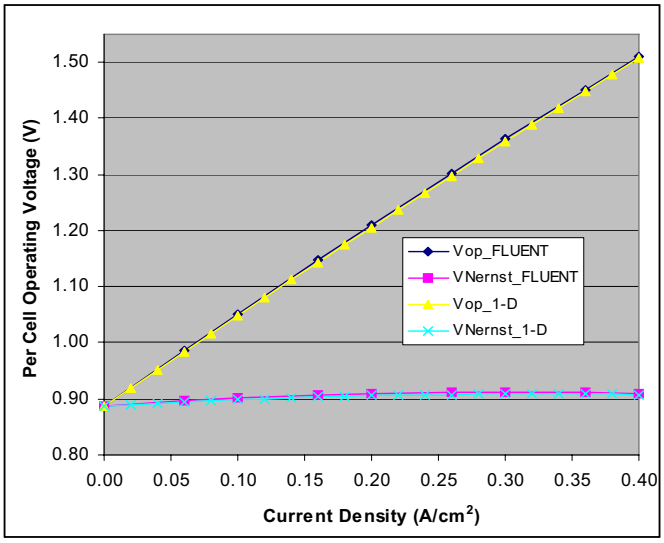


**Figure 3.** Per-cell operating voltage and Nernst potential versus current density for FLUENT model and 1-D model.

Figure 4 shows the outlet mole fractions for the four process gas components versus current density. Note that the mole fractions of $H_2$ and CO increase with current density while the mole fractions of steam and $CO_2$ decrease. Note also that for the conditions chosen, the ratio of produced H2 to CO is about 2-to-1, which is the desirable ratio for syngas. The CO mole fraction predicted by the 1-D model is shown to be the same as the FLUENT predictions. Mole fractions of the $H_2O$, $CO_2$, and $H_2$ for the 1-D model were also essentially the same values as the FLUENT model, but were not plotted.

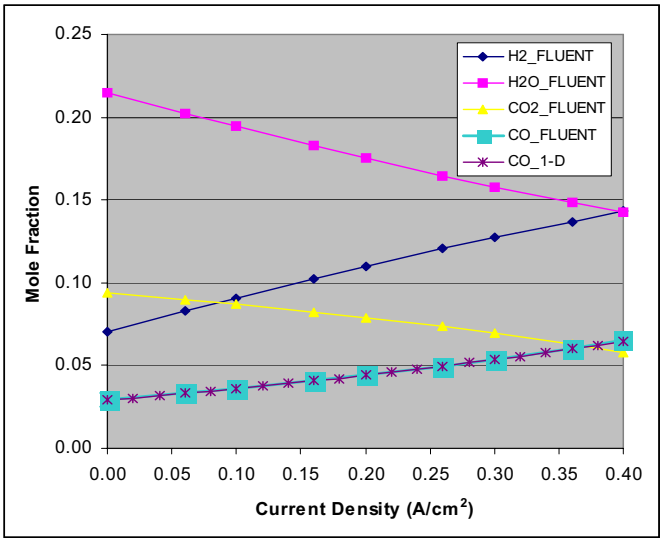


**Figure 4.** Outlet mole fractions versus current density for FLUENT model and 1-D model.

Contour plots of the mole fractions of each process gas component are shown in Figure 5 for a current of $I$ = 25.60 A or a current density of $i$ = 0.4 A/cm$^2$. The top 8 cm in each plot represents the active cell area, while the bottom 35 cm is the adiabatic outlet region. The mean values at the exit correspond to $i$ =0.4 A/cm$^2$ values plotted in Figure 4. As the flow goes through the active cell area, $H_2$ is produced and $H_2O$ is consumed. In the FLUENT model, the $H_2$ then reacts with the $CO_2$ to form CO. At the exit of the active cell area, the composition is not in equilibrium and it continues to react as it flows downstream and comes to equilibrium. Note that $H_2$ is consumed while $H_2O$ and CO are produced in this equilibration region. At this current density, a higher amount of CO is produced on the right side compared with the left side.

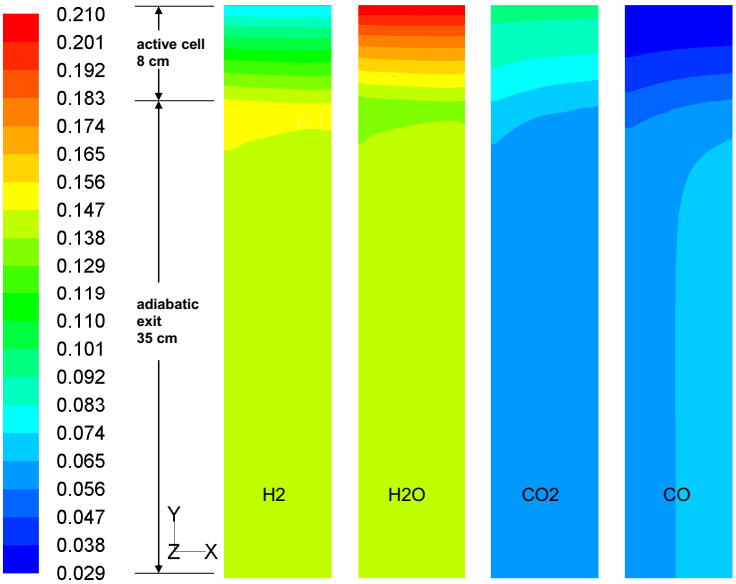


**Figure 5.** Contour plots of mole fractions of $H_2$, $H_2O$, $CO_2$, and CO at i=0.4 A/cm$^2$ for adiabatic FLUENT model in active cell area and outlet region.

Figure 6 shows contour plots of mole fractions of CO for each current density depicted. The color range for each plot is scaled from the minimum value to the maximum value for each current density. For current densities lower than 0.27 A/cm$^2$, the operating voltage is lower than thermal neutral and, with the adiabatic boundary condition; the active cell is hottest in the upper left and coolest in the lower right. The thermal situation is reversed for current densities above 0.27 A/cm$^2$. This temperature variation is responsible for the shift in local relative CO production from highest on the left side at low current density to highest on the right side for high current density. At higher temperature locations, the local Nernst potential is relatively low and therefore the local CO production rate is relatively high. The reverse is true for lower temperature locations.

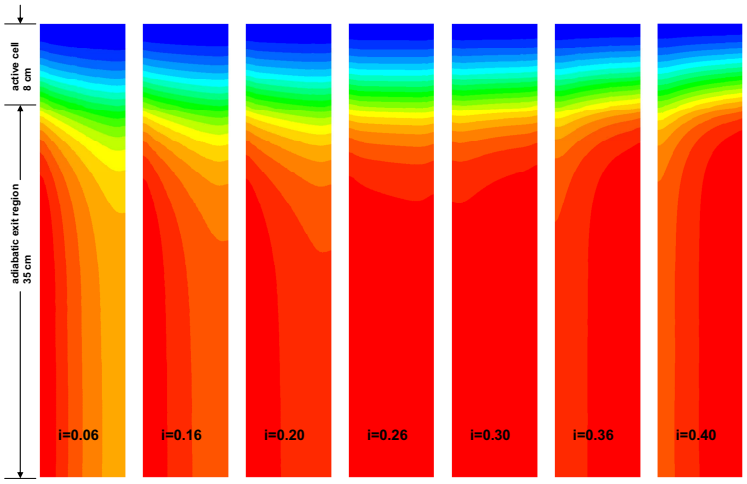


**Figure 6.** CO mole fractions for active cell and outlet region for various current densities (process gas stream flows from top to bottom, air sweep flows from left to right).

Figure 7 shows the total average outlet gas mixture temperature. In the 1-D model, there is only a single temperature predicted at the outlet, for both the process gases and the sweep gas. These two outlet temperature streams can vary up to 10°K in the FLUENT model. To obtain an averaged temperature for the two streams in the FLUENT model, a heat-capacity-rate-average value was used:

$$\overline{T}_{mix,out} = \frac{\sum \dot{m}_i c_{p_i} T_i}{\sum \dot{m}_i c_{p_i}} \qquad (24)$$

where $\dot{m}_i$ is each individual gas component ($H_2O$, $H_2$, $CO_2$, CO, or $N_2$) mass flow rate, and $c_p$ is the specific heat of each gas. The thermal neutral voltage for this case is shown to be about 1.34 V.

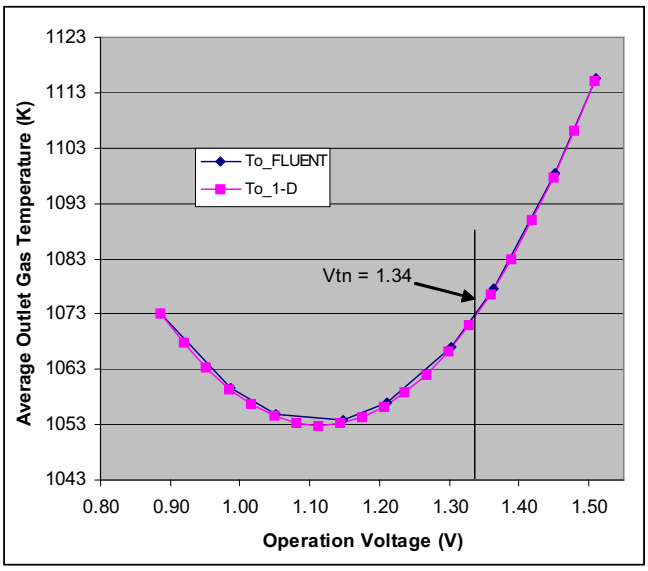


**Figure 7.** Average outlet gas temperature versus operating voltage for FLUENT model and 1-D model.

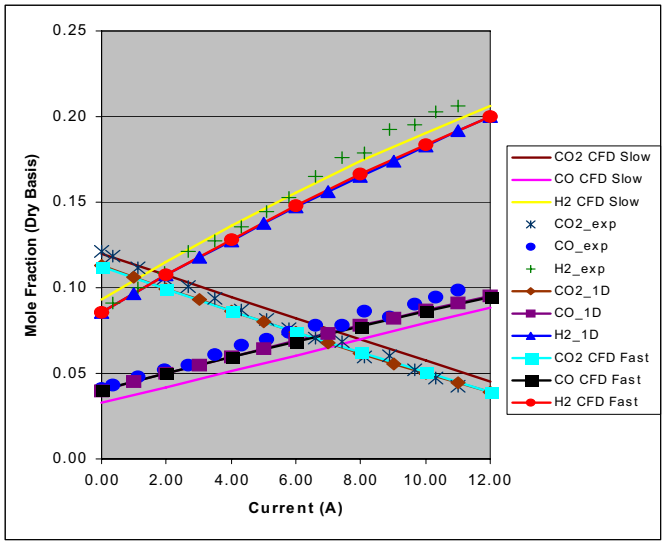


**Figure 9.** Outlet mole fraction versus current for FLUENT model and experiment.

### III.B. FLUENT and Experimental Results

Predictions of the FLUENT model compared to the experimental results are discussed in Figures 8 through 11. Figure 8 shows the per-cell operation voltage versus current polarization curves for the FLUENT model and the experimental results. The contact resistance in the FLUENT model was adjusted so as to obtain the same slope on the V-i curve. A myriad of reasons from Ref. [3] discuss why the experimentally measured open cell potential does not match the theoretical value exactly. Figure 9 shows the outlet mole fraction (dry basis) as a function of current for: (1) FLUENT model with slow cool down, (2) experiment values, (3) 1-D model predictions, (4) FLUENT model with fast cool down. The FLUENT fast cool down and 1-D model predictions are essentially the same. The 1-D model results were obtained at 800°C, so a fast cool-down kinetically freezes the shift reaction at the 800°C composition. The FLUENT slow-cool-down case predicts a lower amount of CO and higher amount of $H_2$ being produced. The experimenters noted that the process gas stream leaving the oven probably cools quite fast and freezes the reaction. This happens since there is a small length (~2-in.) of tubing exposed to room air as it exits the oven, while the remaining length (~50-in) is insulated before sampling at the gas chromatograph. There appears to be a fairly good agreement between these models and the experimental results. Both the FLUENT fast model and the 1-D model under-predict the production of $H_2$ and over-predict the production of CO at higher currents, but are right on at low currents.

Figure 10 shows the FLUENT-predicted mean electrolyte temperature compared to experimentally measured internal stack temperatures as a function of operating voltage. Temperature trends are similar

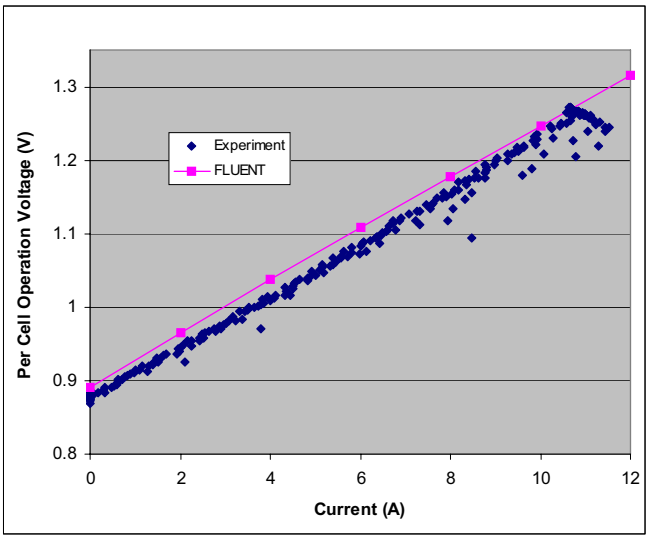


**Figure 8.** Per cell operation voltage versus current for FLUENT model and experiment.

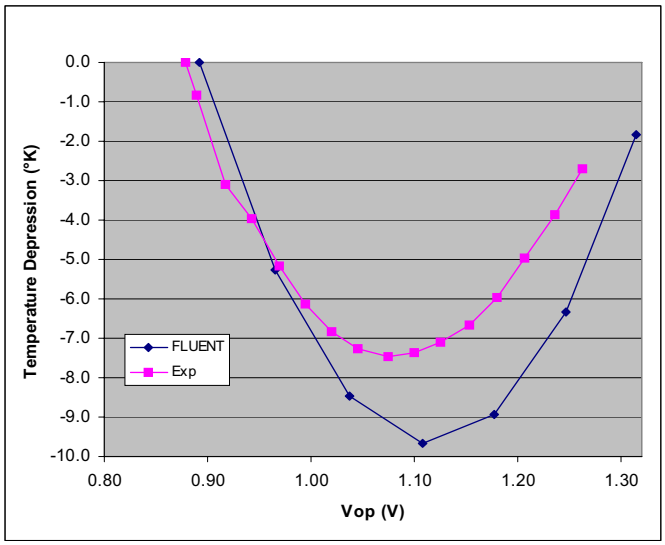


**Figure 10.** Temperature versus Vop for FLUENT model mean electrolyte temperature and experiment.

between the model and the measurements, but the FLUENT model predicts a larger cell-center temperature depression than was measured with the miniature thermocouples inserted into the stack. The difference at the start of the plot is due to the low experimental open cell value as stated above. The FLUENT model does not include radiation heat transfer in the current collector. This would have the affect of increasing the effective thermal conductivity of the current collector if included. The experimental measurements are obtained in a very harsh environment with electrical current flowing through the cell. The possibility also exists that the experimental values were not at steady state. The experimenters are investigating this possibility. This experiment was not run up to thermal neutral voltage.

Figure 11 shows the mole fraction of CO as a function of position for the FLUENT fast and slow cool down models. The inlet composition quickly reacts to equilibrium in the first few centimeters after entering the heated inlet duct and stays there until the active cell area. The CO mole fraction rapidly rises in the cell where the $H_2$ is produced. A length of ~5 cm is required for the composition to come to equilibrium downstream of the active cell region. The fast cool down model shows the temperature (not plotted) of the process gas stream drops to 300 K in over a length of ~1-cm. The slow cool down model only reaches 400 K by the end of the 20 cm length. A mesh sensitivity in this fast cool down region needs to be done since everything is changing so quickly.

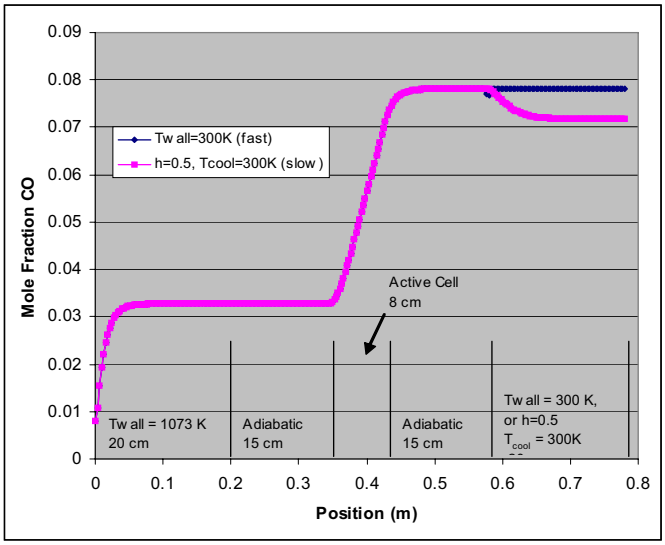


**Figure 11.** Mole fraction CO versus position for fast and slow cooling.

## IV. CONCLUSIONS

A 3-D CFD model has been developed using the FLUENT code, incorporated the thermo-chemical reactions to perform co-electrolysis of steam and $CO_2$ in a solid oxide electrolysis cell (SOEC). A brief description of a 1-D model developed for co-electrolysis and comparisons with the FLUENT model show essentially exact agreement. Both the FLUENT model and the 1-D model are shown to compare quite favorably with experimental results of a co-electrolysis experiment. The FLUENT model created to predict the experiment shows a marked difference in the production of CO and $H_2$ when considering how fast the process gas stream is cooled.

## NOMENCLATURE

| | |
|---|---|
| $ASR$ | area specific resistance, Ω-cm$^2$ |
| $C$ | concentration, mol/m$^3$ |
| $F$ | Faraday constant, 96487 J/V-mol |
| $\Delta G$ | Gibbs free energy, J/mol |
| $\Delta H$ | molar enthalpy reaction, J/mol |
| $h_r$ | radiation heat transfer coefficient, W m$^{-2}$ K$^{-1}$ |
| $i$ | current density (A/cm$^2$) |
| $I_e$ | total ionic current, A |
| $j$ | electrons per transfer |
| $K_{eq}$ | equilibrium constant |
| $k_b$ | backward reaction rate, kmol m$^{-2}$Pa$^{-2}$s$^{-1}$ |
| $k_f$ | forward reaction rate, kmol m$^{-3}$ Pa$^{-2}$ s$^{-1}$ |
| $NNR$ | net reaction rate, kmol m$^{-3}$ s$^{-1}$ |
| $N$ | total molar flow rate |
| $\Delta n_o$ | molar rate of monotonic oxygen |
| $n$ | number of moles |
| $P$ | pressure, Pa |
| $Q$ | external heat transfer, W |
| $R$, $R_u$ | universal gas constant, 8314 J/kgmol-K |
| $T$ | temperature, K |
| $T_w$ | outer wall temperature, K |
| $T_\infty$ | oven temperature, K |
| $V$ | volume, m$^3$ |
| $V_n$ | open cell Nernst potential, V |
| $V_{tn}$ | thermal neutral voltage, V |
| $V_{op}$ | operation voltage, V |
| $W$ | work, product of V*I, W |
| $y$ | mole fraction |
| $\varepsilon$ | emissivity |
| $\sigma$ | Stefan-Boltzmann constant |

Subscripts

| | |
|---|---|
| $H_2$ | Hydrogen gas |
| $H_2O$ | steam |
| $CO_2$ | carbon dioxide gas |
| $CO$ | carbon monoxide gas |
| $o$ | open-cell |
| $O_2$ | oxygen |
| $p$ | products |
| $r$ | reactants |
| $Std$ | standard pressure |
| $tn$ | thermal neutral |
| $eq$ | equilibrium |
| $t$ | thermal |

**ACKNOWLEDGEMENTS**

This work was supported by the Idaho National Laboratory, under DOE Laboratory Directed Research and Development program and the U.S. Department of Energy, Office of Nuclear Energy, Nuclear Hydrogen Initiative Program. The Idaho National Laboratory is operated by the Battelle Energy Alliance through DOE Contract DE-AC07-05ID14517.

**REFERENCES**

1. C.M. Stoots, J.E. O'Brien, G.L. Hawkes, J.S. Herring, and J.J. Hartvigsen, "High Temperature Co-Electrolysis of H2O and CO2 for Syngas Production," *2006 Fuel Cell Seminar*, Honolulu, Hawaii, Nov. 13-17, 2006, paper no. 418.
2. G.L. Hawkes, J.E. O'Brien, C.M. Stoots, R. Jones, "Three Dimensional CFD Model of a Planar Solid Oxide Electrolysis Cell for Co-Electrolysis of Steam and Carbon-Dioxide," *2006 Fuel Cell Seminar*, Honolulu, Hawaii, Nov. 13-17, 2006, paper no. 298.
3. C.M. Stoots, J.E. O'Brien, J.J. Hartvigsen, "Test Results of High Temperature Steam/CO2 Coelectrolysis in a 10-cell Stack," *Nuclear Hydrogen Embedded Topical Meeting, ANS Annual Meeting*, Boston Massachusetts, June 24-28, 2007 (accepted).
4. J.E. O'Brien, C.M. Stoots, G.L. Hawkes, J.S. Herring, and J.Hartvigsen, "High-Temperature Co-electrolysis of Carbon Dioxide and Steam for the Production of Syngas; Equilibrium Model and Single-Cell Tests," *Nuclear Hydrogen Embedded Topical Meeting, ANS Annual Meeting*, Boston Massachusetts, June 24-28, 2007 (accepted).
5. FLUENT version 6.3.26, Fluent Inc., Lebanon NH
6. G. L. Hawkes et. al., "CFD Model of a Planar Solid Oxide Electrolysis Cell for Hydrogen Production from Nuclear Energy", Paper LOG # 326, *NURETH-11* , Popes Palace Conference Center, Avignon, France, October 2-6, 2005.
7. Lehnert, et. al., "Modeling of gas transport phenomena in SOFC anodes", *Journal of Power Sources*, 87, 57-63, 2000
8. "Fuel Cell Handbook", DOE NETL, Morgantown WV, 2004